Post Porosity Plasma Protection: Scaling of Efficiency with Porosity

*Theo Frot, Willi Volksen, Sampath Purushothaman, Robert L. Bruce, Teddie Magbitang, Dolores C. Miller, Vaughn R. Deline, and Geraud Dubois**

Increasing the porosity of oxycarbosilane dielectrics is a key approach to lower the interconnect signal delay and thus enable manufacturing of lower power consumption and higher performance microprocessors. However, this path leads to excessive dielectric process damage as the industry adapts procedures developed for dense and microporous insulators to mesoporous materials. Currently ultralow dielectric constant (*k*) materials cannot be integrated at the most aggressive pitch. Here, it is reported that the post porosity plasma protection enables the mitigation of process damage across a wide range of porosity regimes. The exponential increase in plasma damage with porosity when going from microporous $k = 2.4$ to mesoporous $k = 1.8$ is shown. Using the same range of materials, the strategy allows a reduction in process damage to a constant minimal level on both blanket wafers and patterned structures. The results demonstrate how the strategy can enable the extendibility of current materials and processes to future technology nodes.

1. Introduction

In recent years, the emergence of low power consumption/high performance microprocessors has been possible due to the reduction of device dimensions in parallel with the introduction of low dielectric constant (*k*) materials.[1,2] To continue along this pathway, the strategy adopted by the microelectronics industry has been to initially migrate from silicon oxide type dielectrics to lower *k* organosilicates and then to continuously add porosity to organosilicate low-*k* materials. This ideal trend is now questionable due to the technical difficulties in integrating highly porous $k \leq 2.4$ materials, a critical concern for large-scale integration. Consequently, the semiconductor industry is considering maintaining the same *k* or even backtracking to slightly higher *k* values (2.55 and/or 2.7) when going to smaller device dimensions.[3] In general, materials with $k \sim 2.4$-2.6 can be obtained by deposition of organosiliane-based precursors, with a pore size distribution limited to below 2 nm (**Figure 1**).[2] To reach $k < 2.4$, addition of a separate porogen is usually required.[2,4] This results in a modification of the dielectric material backbone during plasma enhanced chemical vapor deposition (PECVD) and an increase in the average pore size, range of pore sizes in the pore size distribution as well as pore interconnectivity.[5–8] For instance, the emergence of mesoporosity (pore diameter > 2 nm) can be observed for materials with $k \leq 2.2$. This increase in pore size and pore interconnectivity with decreasing *k*, i.e. increasing porosity, exacerbates integration issues, such as, etch profile non-uniformity, increase in integrated *k* due to plasma induced damage and overall deterioration of electrical reliability.

As of today, the different solutions proposed to minimize process damage have had limited success: organic or metallic hard-mask integration,[9] low temperature plasma etch,[10] post plasma damage repair,[11] post-integration porogen removal.[12] The last example suffered from up to 10% shrinkage during porogen burnout.[13] As a result, the use of high carbon content and ultramicroporous materials appears to be the preferred path of the industry.[5] Unfortunately, this approach has led to mixed results and increasing development costs, as new ultralow-*k* (ULK) materials have to be designed for each technology node.

We recently introduced an alternative strategy, post porosity plasma protection (P4),[14,15] which takes advantage of the increasing pore size and interconnectivity when the dielectric constant is decreased below 2.4. This strategy consists of protecting the fully cured porous ULK material by filling the pores with a sacrificial agent and then integrating this composite non-porous dielectric.[16] Subsequent thermal removal of the pore filler following the most damaging process steps regenerates the material to its original porous state. We previously demonstrated the potential of this strategy by protecting a porous material, $k = 2.0$, from plasma damage using various organic polymers. Here, we report that our approach can be applied to a wide range of porous materials as demonstrated with a family of spin-on ULK dielectrics spanning the microporous and mesoporous regime, i.e. $k = 2.4$ to 1.8. In this respect, the proposed

Dr. T. Frot, Dr. W. Volksen, T. Magbitang, D. C. Miller, V. R. Deline, Dr. G. Dubois
IBM Almaden Research Center
650 Harry Rd., San Jose, CA 95120, USA
E-mail: gdubois@us.ibm.com
Dr. S. Purushothaman, Dr. R. L. Bruce
IBM T. J. Watson Research Center
1101 Kitchawan Rd., Rte 134,
Yorktown Heights, NY 10598, USA

DOI: 10.1002/adfm.201200152

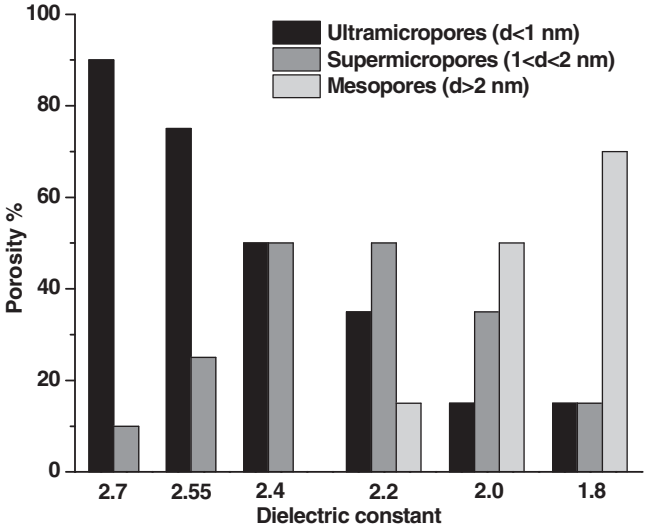

Figure 1. Evolution of porosity in typical low-*k* materials as a function of *k*.

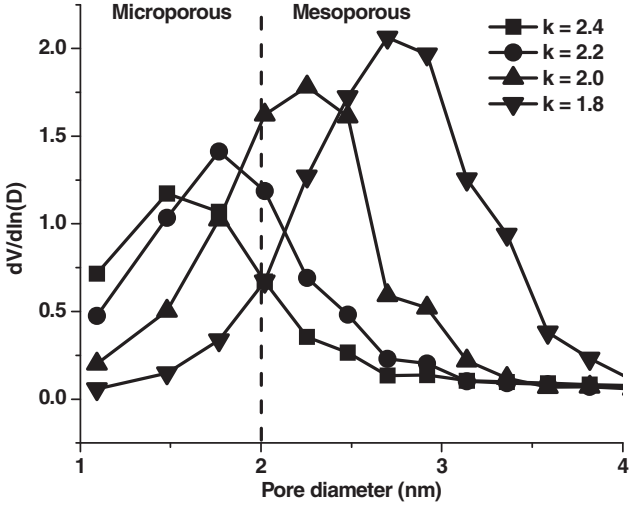

Figure 2. Pore size distribution of ULK films used in this study: $k = 2.4$ (■), $k = 2.2$ (●), $k = 2.0$ (▲), and $k = 1.8$ (▼).

protection strategy addresses both current manufacturing needs as well as enabling extendibility to future technology nodes.

2. Results and Discussion

2.1. Matrix and Filler Selection

Based on our experience with spin-on organosilicates, we selected a manufacturing grade spin-on resin derived from an ethylene-bridged organosilicate precursor (Si-CH_2-CH_2-Si backbone).[17–19] The sol-gel chemistry was tuned to generate an intrinsically porous $k = 2.4$ film, without the use of an additional pore generator (porogen).[20] Further lowering of *k* was achieved by generating additional porosity via a classical nucleation and growth approach employing a polymeric porogen.[19] In the ensuing discussion, films are identified by their dielectric constant, e.g. ULK-2.4 is a film with $k = 2.4$.

The properties of ULK-2.4 to ULK-1.8 are detailed in **Table 1**. The density and Young's modulus (E) were measured by x-ray reflectivity (XRR) and surface acoustic wave spectroscopy (SAWS), respectively. The ethylene-bridged backbone provides superior mechanical properties (cf. Table 1) as compared to poly(methylsilsesquioxanes) leading to highly porous ULK films sufficiently robust to withstand integration conditions.[21,22] The film porosity and pore size distribution were determined by toluene ellipsometric porosimetry (EP) on thin films,[23] using the Kelvin model. ULK-2.4 is microporous with the lower dielectric constant candidates exhibiting progressively increasing percentages of mesopores and approaching fully mesoporous character for ULK-1.8 (cf. **Figure 2**).

As previously reported,[15] different polymeric fillers (sacrificial agents) were selected based on the following criteria: i) low molecular weight (MW), ii) low glass transition temperature (T_g) and low viscosity above T_g to facilitate pore filling, iii) compatibility with integration processes (stable up to 300 °C in inert atmosphere), iv) complete decomposition under back-end-of-the-line (BEOL) compatible conditions, and v) efficient ULK protection during the aggressive integration steps. In this study, we used proprietary methacrylate based copolymers (PMA) with thermal properties meeting criteria (iii) and (iv) (*vide supra*) and identified by their molecular weight (for example, PMA-1.1 is a PMA copolymer with a molecular weight of 1,100 daltons).

Table 1. Physical properties as a function of porosity of ULK films employed in this study.

Film	*k*	Density [g cm^{-3}]	*E* [GPa]	Porosity %
ULK-2.4	2.4	1.165	9.2	23%
ULK-2.2	2.2	1.090	7.0	27%
ULK-2.0	2.0	0.978	4.8	33%
ULK-1.8	1.8	0.804	2.4	46%

2.2. Pore Filling

We developed and optimized pore filling protocols using the films and polymers described in Section 2.1. A three step process was employed to obtain filled ULKs with negligible polymer excess on top: i) spin-coat a polymer containing solution on top of the ULK, ii) heat the system above the polymer's T_g in order to allow filling of the pores by capillary action, and iii) removal of the polymer excess (overburden) using a solvent wash.[24] This overburden removal is critical as it not only facilitates the ULK characterization but also provides a clean ULK surface for good hardmask adhesion, a key prerequisite for integration. All characterization of filled films reported here are on samples where the overburden was removed.

2.2.1. Fill Optimization

We developed industry compatible protocols in order to obtain etch profiles using 200 mm wafers. As a prerequisite, polymer fills had to be both homogeneous throughout the ULK thickness and uniform across the wafer plane. In this respect, optimization of the fill protocol to yield ULK/polymer composite films with the desired characteristics was mandatory.

The main issue encountered during filling was the uneven distribution of the filler throughout the ULK thickness. We observed that the spectral reflectometry (SRM) data did not correspond to a single-layer system but to a superposition of layers with varying refractive indices (RI). Similarly, the XRR data indicated a density gradient through the thickness of the film. In both cases, variations in density or RI indicate a non-uniform polymer fill. Typically, this issue can be resolved by increasing the filling temperature and/or time.[24] As we had to limit the fill time to a few minutes (for industry compatibility), we decided to increase the post-apply bake (PAB) temperature while staying in the range where the polymer is thermally stable.

Unfortunately, significant temperature increases above T_g can lead to de-wetting of the fill polymer on the ULK film surface. In turn, this causes polymer to puddle on top of the ULK, precluding uniform polymer filling. Although, de-wet can be prevented by modifying the substrate surface,[25] grafting the polymer strands on the substrate,[26] or adding nanoparticles to the polymer,[27] these solutions are not compatible with current semiconductor process requirements. We solved the de-wetting issue through proper choice of the PAB temperature and adding surfactants to the filler solution in order to enhance the polymer's wettability.

2.2.2. Fill Characterization

Great emphasis was placed on the complete characterization of the ULK/polymer composite systems in order to verify effective pore filling by the polymer and to assess the fill level. We will first detail the characterization of the filled films and then proceed to discuss a ULK-2.0 filling example.

As previously mentioned,[15] we used a combination of techniques to characterize the filled ULK, such as SRM, XRR, depth profiling by X-ray photoelectron spectroscopy (d-XPS), depth profiling by secondary ion mass spectrometry (d-SIMS), ellipsometric porosimetry (EP) and Fourier transform infrared spectroscopy (FTIR). SRM was used as a first pass evaluation of the filled ULK. An increase in the refractive index (RI) of the film indicates that the polymer has filled the porosity as air (RI ≈ 1) is replaced by polymer (RI ≈ 1.5). Knowing the ULK's RI (RI_{ULK}), the polymer's RI (RI_{poly}) and the porous fraction of the ULK (v), it was possible to estimate the fill percentage (F) of the ULK's porosity by the polymer from the RI of the filled ULK ($RI_{f\text{-}ULK}$):

$$RI_{f-ULK} = RI_{ULK} + \upsilon \times F \times (RI_{poly} - RI_{air}) \quad (1)$$

The fill homogeneity was also qualified by verifying whether the SRM spectrum corresponds to a single layer film and the total thickness is equivalent to that of the pristine film. A slight shrinkage of the ULK (~2%) is observed after polymer fill.

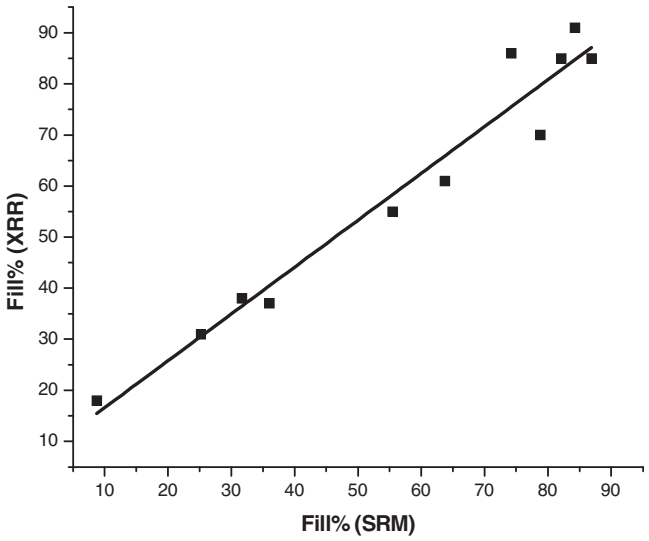

Figure 3. Comparison of Fill% as determined by XRR and SRM for ULK-2.2/PMA-1.1

The contraction of the ULK is most likely a result of the capillary forces exerted by the polymer on the surrounding matrix, similar to observations reported for EP.[23] One must note that the shrinkage we observe is prior to integration of the dielectric film, whereas in the post-integration porogen removal the shrinkage occurs after integration.[12,13] Subsequent expansion of the film during pore filler burnout could be an issue, but preliminary results on single damascene integration suggest this is not the case as we do not observe any delamination.

XRR was used to obtain a more accurate analysis of the polymer fill (level and homogeneity). The XRR scans of the filled ULK can be fitted using a multilayer model of varying density and thickness. Knowing the ULK's density (ρ_{ULK}) and the polymer's density (ρ_{poly}), it was possible to estimate the Fill% (F) from the density of the filled ULK ($\rho_{f\text{-}ULK}$):

$$\rho_{f-ULK} = \rho_{ULK} + \upsilon \times F \times \rho_{poly} \quad (2)$$

If the fill is not homogeneous, significant perturbations of the XRR scans are observed,[27] this will be detailed in the example below. In general, we considered the fill as homogeneous if the XRR data could be fitted using a single-layer model. **Figure 3** compares the Fill% as determined by XRR and SRM for ULK-2.2/PMA-1.1 system, indicating good agreement between the two techniques. Surprisingly, fill levels approaching 90% can be achieved for even microporous materials (ULK-2.2), using a low molecular weight polymer.

2.2.3. Case Study: ULK-2.0 Filling

For the case of a ULK-2.0/PMA-4.7 composite system, we will demonstrate to the reader how the various characterization techniques allowed the optimization of fill conditions while providing the data to validate our homogeneous fill model. The SRM and XRR analyses of the pristine ULK-2.0 film are given in **Figure 4**. SRM indicates a film thickness of 524 nm with a RI = 1.298, while XRR provides an almost equivalent thickness

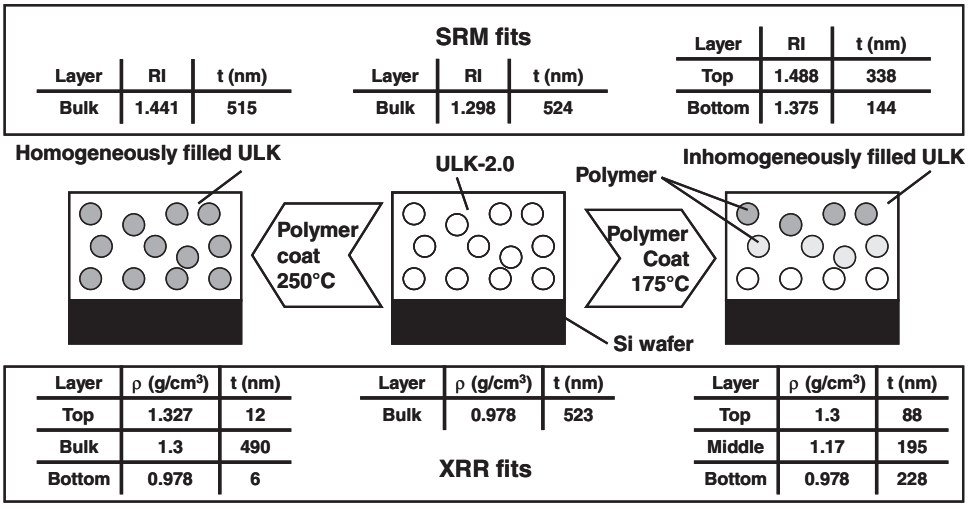

Figure 4. Schematic of the ULK-2.0/PMA-4.7 composite system: middle–pristine, left–homogenous fill, right–inhomogeneous fill and corresponding SRM and XRR fitting data.

of 523 nm and a density of 0.978 g.cm^{-3}. For a single layer film, the two techniques give consistent thickness measurements.

In order to fill the ULK-2.0, we first spin-coated a solution of PMA-4.7 on top of the ULK-2.0 to fully cover the surface. The wafer was then heated at 175 °C, cooled to room temperature, and the remaining PMA-4.7 overburden was removed using a 1-methoxy-2-propanol (PMOH) solvent wash. The SRM data (Figure 4) can be fitted with a minimum of 2 layers, where the top layer has a thickness of 338 nm and a RI of 1.488 and the underlying layer has a thickness of 144 nm and a RI of 1.375. This indicates the top region of the film with the significantly higher RI is more filled. Fitting of the XRR data supports this conclusion. Here, the film can be modeled using a minimum of three layers, which are 88, 195 and 229 nm thick and have densities of 1.3, 1.17 and 0.978 g.cm^{-3}, respectively, with the 88 nm layer being on top. This variation in density leads to Kiessig fringes appearing near the critical angle of the XRR scan (**Figure 5**). The top regions of the film are denser than the ones closer to the substrate, i.e. the fill level decreases through the thickness of the ULK-2.0. SRM and XRR analyses both point toward an inhomogeneous polymer fill.

As detailed in 2.2.1, a more homogeneous fill can be obtained by using a higher PAB temperature. By switching to a PAB temperature of 250 °C and removing the overburden, SRM analysis of the resulting composite film using a single layer fit gave a film thickness of 515 nm and a RI = 1.441. The increase in RI is consistent with a quasi-complete filling of the porosity of the ULK (according to Equation 1). As mentioned previously, a slight shrinkage (~2%) is observed. Fitting of the XRR data confirms the observation made by SRM. Even though the filled film is modeled using a 3-layer system, it must be noted that the bulk layer represents more than 95% of the ULK-2.0's thickness and the XRR scan resembles that of a single-layer film. Indeed, the XRR scan has a well-defined critical angle and regular Kiessig fringes (Figure 5). The top and bottom layers used here are thin (< 13 nm). While the denser top layer is most likely due to the slightly over-filled film surface, the less dense layer

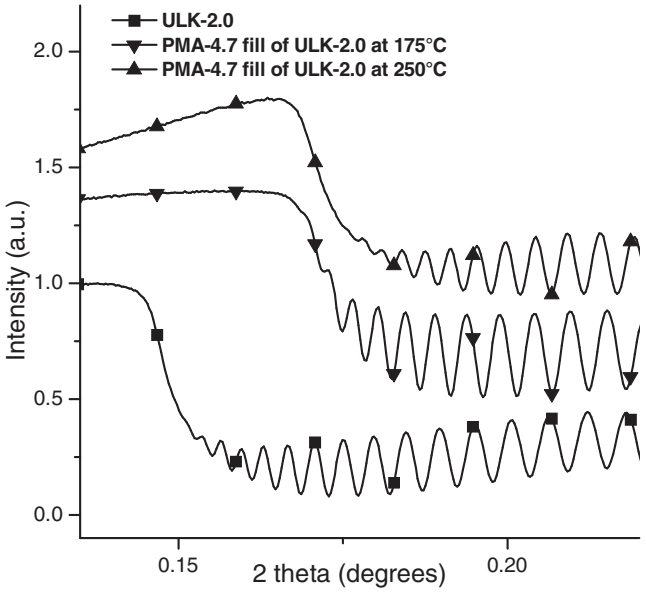

Figure 5. XRR scans of ULK-2.0: pristine (■), inhomogeneously filled at 175 °C (▼), and homogeneously filled at 250 °C (▲) with PMA-4.7.

at the bottom interface may be due to a less accessible porosity or an artifact of the fitting program. For all practical purposes, the filled ULK-2.0 is a single layer film according to XRR. The film is 508nm thick and has a density ρ = 1.297 g.cm^{-3}, which corresponds to a fill of 84% (from Equation 2 using $\rho_{PMA\text{-}4.7}$ = 1.05 g.cm^{-3}).

The ULK-2.0 filled at 250 °C was further characterized using d-SIMS and d-XPS in order to complement the SRM and XRR analyses and obtain compositional information. **Figure 6**a represents a log-plot of the C/Si ratio as a function of cesium ion sputtering time (depth) as obtained by SIMS. A thin layer of Pt was deposited on the surface to reduce surface charging

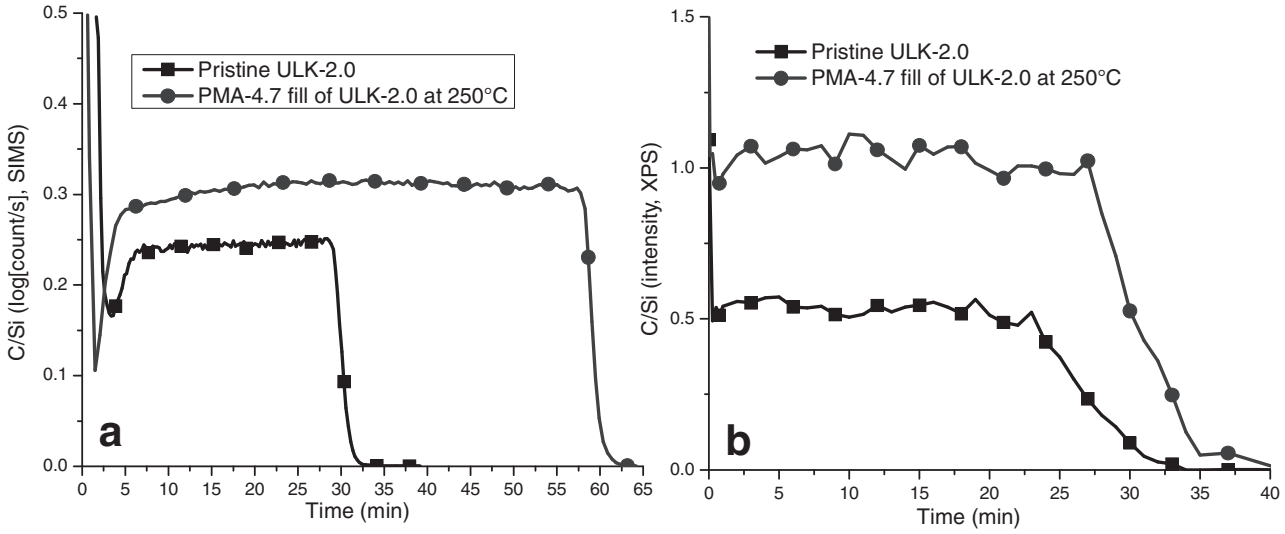

Figure 6. C/Si ratio as a function of sputter time of pristine (■) and polymer filled (●) ULK-2.0 analyzed by: a) SIMS and b) XPS.

during the SIMS measurement; therefore, the first 5 min of sputtering time may be disregarded. Three major conclusions can be drawn from the d-SIMS. First, total sputtering times of 60 min and 30 min for the filled and pristine film, respectively, suggest the filled material is more dense and more carbon rich. Second, the C/Si ratio is significantly higher for the filled film, consistent with the addition of a non-silicon, carbon rich component. Third, the C/Si ratios are constant as a function of sputtering time for both filled and unfilled films, indicating a homogeneous composition which implies a homogeneous fill. The same three observations made on the d-SIMS hold true for the d-XPS (Figure 6b). For both these techniques, one must keep in mind that the C/Si ratio is not an absolute measure, but gives an indication of variations in trend. The true C/Si ratio of our pristine ULK films measured by XPS, electron energy loss spectroscopy and Rutherford backscattering falls between the values of 0.5 and 0.8 from one measurement to another. We can conclude that both techniques validate the XRR and SRM analyses, i.e. the ULK-2.0 is homogeneously filled.

2.3. Protection Evaluation

In addition to the ongoing work on fill optimization, we evaluated the P4 protection effect on blanket wafers using the plasma induced damage (PID) test.[15] Filled and pristine samples are exposed to standard ULK strip chemistry,[28,29] selected to simulate complete removal of about 300 nm of HM8006 (from JSR Micro) organic planarization layer. This creates a dense SiO_2-like layer in the top region of the ULK film, which is removed using a dilute hydrofluoric acid (DHF) dip, which does not dissolve the undamaged hydrophobic bulk of the film. Finally, a 400 °C polymer burnout under N_2 is performed. In an ideal case, i.e. no process damage, no thickness loss would be observed and the corresponding PID would be zero. However, under real process conditions, this leads to a loss of ULK thickness and an associated PID expressed in nanometers. As predicted, the PID of the protected films is systematically less than that of the corresponding pristine film. The plasma damage created here represents what happens at the bottom of the trench and not on the sidewalls as the etch ions and radicals are going parallel to the sidewalls and damage them much less than the trench bottom.[30]

2.3.1. Influence of the Fill Polymer on the PID Reduction

We studied the influence of the polymer's fill level, nature and MW on the PID. We previously showed that the PID decreases linearly as the fill level increases,[15] and also demonstrated that, at similar fill levels, certain polymers offer more protection than others. However this increased plasma protection does not appear to stem from an increase in plasma resistance of the polymer. Polymers with aromatic structures and/or increased carbon contents, which usually have better plasma resistance,[31] do not offer enhanced plasma protection using the P4 approach. For example, polystyrene offers similar protection to the PMA-type polymer even though it has more aromatic structures and a higher carbon concentration.

The last point of the polymer study was to see whether its MW had an influence on the PID reduction. We filled at approximately 90% a mesoporous ULK-1.8 with the PMA-type polymer at 4 different molecular weights (2700, 4700, 7200 and 10000 daltons), and then performed a PID evaluation. The plasma damage suffered by the protected samples is similar (less than 5nm variation) and significantly lower than the PID of the unprotected sample. Therefore, the polymer's MW does not seem to have an impact on the PID.

2.3.2. PID Reduction as a Function of Porosity

We also studied the PID as a function of the film porosity while maintaining a constant matrix composition. Indeed sol-gel chemistry enables us to obtain porous, low-k spin-on materials with constant matrix composition. This is different from PECVD

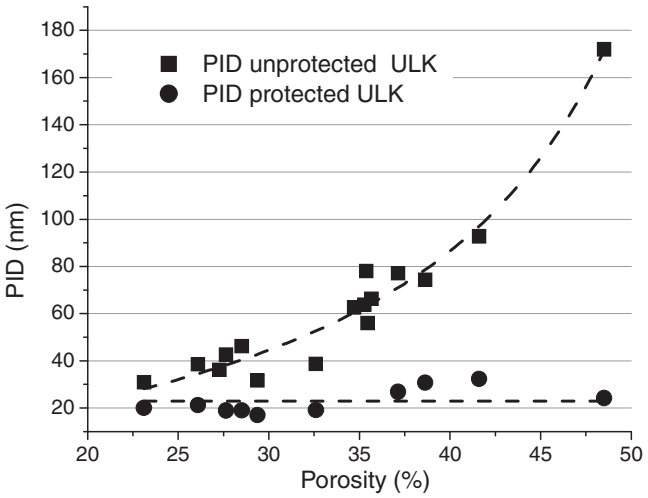

Figure 7. PID of unprotected (●) and protected (■) ULK films as a function of porosity.

where variations in the nature or quantity of the porogen lead to modifications of the matrix chemical composition.[32] We ran the PID tests on both protected and pristine (unprotected) ULK with k values ranging from 1.8 to 2.4 (porosity spanning from microporous to mesoporous). **Figure 7** illustrates the observed PID as a function of porosity for pristine films and films protected with PMA-1.1.

The PID of the unprotected ULK increases exponentially with porosity. This is a direct consequence of the increase in porous volume, pore size distribution (Figure 1) and pore interconnectivity.[5] As a result of this increase, ions and radicals from the plasma can more easily penetrate the material leading to greater and deeper damage. This underlines the limiting factor when trying to integrate highly porous materials. This trend in increasing plasma damage explains why the semiconductor industry has great difficulty in integrating ULK materials at the most aggressive pitch.

On the other hand, the protected ULK exhibits a constant damage (PID) of approximately 20 nm, irrespective of porosity. It is well known that films with a higher carbon content are more resistant to plasma damage.[33] Here, we are comparing composite films (ULK + polymer) which have very different composition: the lower k filled films have a higher carbon content than the higher k filled films. Thus, the behavior of filled films with different carbon and matrix backbone ratio couldn't be anticipated and the constant plasma damage was surprising. In general, this result confirms that highly porous materials can be effectively protected using the P4 approach. Furthermore, the PID is independent of porosity and the filled films behave as if they were non-porous. Irrespective of the type of porosity (microporous to mesoporous and $k = 2.4$ to $k = 1.8$, respectively) the protected ULKs are equally insensitive to plasma damage.

2.4. Etch Profiles

Using optimum fill conditions, trench only single damascene structures were fabricated on 200 mm wafers using a process sequence that limited the post film fill processing steps to a temperature less than 300 °C. A side-by-side comparison of ULK-2.2, ULK-2.0 and ULK-1.8 unprotected or protected by the PMA-1.1, PMA-4.7 and PMA-10, respectively, was performed by cross-sectional scanning electron microscopy (XSEM). The profiles after the dielectric etch, strip, cap open and DHF dip are illustrated on **Figure 8**. The DHF step is used to remove the silica-like hydrophilic damage layer on the trench sides and bottom, a standard process in the microelectronic industry.

No further integration could be pursued on the trench profiles of the unprotected ULKs due to their low quality. The bottom of the line is pitted and microtrenches can be seen at the bottom corners. Moreover, the profile is bowed, an undercut is visible under the hardmask and the critical dimensions (CD, 250 nm lines and spaces) of the line are not maintained because of plasma damage. Furthermore, the damage increases exponentially with increasing porosity, consistent with the PID test on blanket wafers. The measured ULK line to line spacing at half-height decreases from a target value of 250nm to 230 nm for ULK-2.2, 190 nm for ULK-2.0 and 105 nm for ULK-1.8.

In contrast, the profiles using the protected ULKs are of very good quality, using the same processing conditions without any process optimization (e.g. different etch chemistry, dielectric repair).[11] All three profiles present straight sidewalls with good CD control. The trench bottoms are slightly rounded but are devoid of pitting or microtrenching. The line dimensions remain constant when using the P4 strategy, regardless of the porosity. The nominal ULK line width and spacing at half-height for all three ULKs is 250 nm. No blowout of the trench dimension is observed for the protected ULKs, even though we used the same strip chemistry as in Section 2.3 (PID evaluation) which is fairly damaging but emphasizes the difference between pristine and protected porous materials. For very aggressive ground-rules, low-damage optimized strips are used and we expect the damage to be less than 1 nm when working with 20 nm line and space.

To the best of our knowledge, this is the first time such well-controlled line profiles have been observed in such highly porous ULK films (albeit at relaxed ground rules) without extensive process optimization. More importantly, the ability to maintain such tight CD control at $k = 1.8$ even with highly

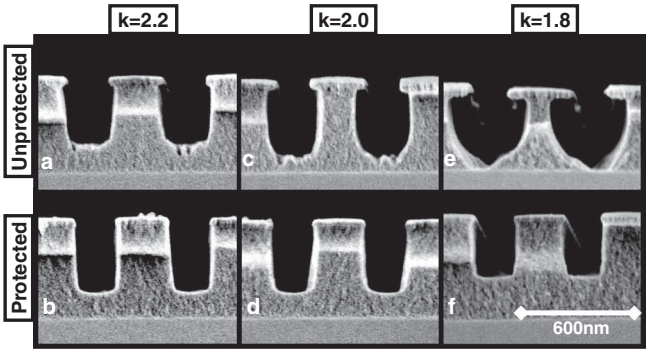

Figure 8. XSEM trench profile after main etch strip, cap open and DHF dip of a) ULK-2.2, b) protected ULK-2.2, c) ULK-2.0, d) protected ULK-2.0, e) ULK-1.8, and f) protected ULK-1.8.

optimized, non-damaging plasma conditions, has never been reported suggesting that the P4 methodology could enable an increased processing latitude for ULK films all the way down to a k of 1.8.

3. Conclusion

We investigated the efficacy of the P4 strategy as a function of porosity. A standard PID test was run on blanket porous thin films with identical matrices and varying porosities (from microporous $k = 2.4$ to mesoporous $k = 1.8$). The damage suffered by the unprotected films increased exponentially with increasing porosity, whereas the PID of the protected films was constant, regardless of level or type of porosity. The same behavior was observed during trench etching of ULKs with a dielectric constant ranging from 2.2 to 1.8. The profile defects using the non-protected films, once again, increased dramatically with the level of porosity, precluding further integration. Using the P4 approach, high quality trench profiles were obtained independent of the level or type of porosity, demonstrating the efficacy of the P4 strategy. In addition, this strategy also provides a method to evaluate the plasma resistance of low-k matrix chemical composition independent of the porosity effect.

We anticipate that the P4 strategy could radically impact the microelectronics industry in two ways to ensure both materials and process extendibility over several generations of processors. First, since it provides the first insights into the relationship of backbone chemistry and materials plasma resistance, the P4 strategy can offer guidance in the design of optimized ULK materials adapted to several technology nodes, eliminating the need for their constant redesign. Second, the P4 strategy enables the integration of highly porous materials using current manufacturing integration schemes and thus ensures process and tooling generational extendibility. Both of these advantages could help the microelectronics industry to control their agenda with regards to new technology nodes and decrease in dielectric constant.

4. Experimental Section

Thin Film Preparation: Porous ULK films were obtained by first spin-coating manufacturing grade oxycarbosilane formulations on 200 mm wafers and then curing at 400 °C under deep ultraviolet irradiation for 7 min.

Spectral Reflectometry: Film thicknesses and refractive indices were measured using a Filmetrics F20 spectral reflectometer. Refractive indices are given for a wavelength of 623.8 nm.

Specular X-Ray Reflectivity: Measurements were used to determine samples density and these were performed using a diffractometer (X'Pert Pro MRD, PANalytical) with ceramic x-ray tube (wavelength = 0.154 nm) and high resolution horizontal goniometer (reproducibility +/–0.0001 degree). XRR data was fitted using X'pert Reflectivity 1.0 by PANalytical B.V.

XPS: XPS analysis was done on a Physical Electronics Quantum 2000 ESCA Microprobe with a monochromatic Al Ka source, using charge neutralization. Depth profiling was done using 4 keV Ar^+ ions, 15 nA, 3 × 3 mm raster. High resolution (58.7 eV pass energy, 0.5 eV/step) scans were taken using a 200 m spot at 45° angle between the sample and the analyzer axis.

SIMS: A Cameca SC-Ultra SIMS instrument was used to acquire the SIMS depth profiles. A 2 keV Cs^+ beam at 3.3 nA provided the sputtering and Cs attached secondary ions of CsC^+, CsO^+ and $CsSi^+$ were detected. A thin layer of Pt, deposited on the surface, and an electron beam at 5 kV were used to mitigate surface charging.

PID Evaluation: Films were subjected to an oxygen containing resist strip chemistry with etch time selected to simulate complete removal of about 300nm of HM8006 organic planarization layer, and dipped in a 1/300 wt diluted HF (DHF) solution in water for 60 s. Films were washed with deionized water and cured at 400 °C under N_2 for 1 h.

Integration Studies: A titanium nitride hard mask (25 nm) was deposited by reactive sputter deposition at room temperature. A low temperature silicon oxide (LTO) top hard mask was also employed to enable resist rework capability. A fluorocarbon containing plasma etch recipe was used to achieve pattern transfer into the ULK layer. Ashing of organic planarization layer or resist layer was performed using a two stage ULK strip.

Acknowledgements

The authors thank all collaborators at IBM, especially Michael Lofaro, and JSR Micro for providing materials.

Received: January 17, 2012
Published online: April 17, 2012

[1] *International technology Roadmap for Semiconductors 2011 Edition*, **2011**, http://www.itrs.net/ (accessed April 2012).
[2] W. Volksen, R. D. Miller, G. Dubois, *Chem. Rev.* **2010**, *110*, 56.
[3] T. Frot, W. Volksen, T. Magbitang, S. Purushothaman, R. L. Bruce, S. Cohen, M. Lofaro, G. Dubois, *Future Fab. Int.* **2011**, *39*, 67.
[4] A. Grill, V. Patel, *Appl. Phys. Lett.* **2001**, *79*, 803.
[5] S. M. Gates, G. Dubois, E. T. Ryan, A. Grill, M. Liu, D. Gidley, *J. Electrochem. Soc.* **2009**, *156*, G156.
[6] E. Huang, M. Toney, W. Volksen, D. Mecerreyes, P. Brock, H. Kim, C. Hawker, J. Hedrick, V. Lee, T. Magbitang, *Appl. Phys. Lett.* **2002**, *81*, 2232.
[7] A. Urbanowicz, K. Vanstreels, P. Verdonck, D. Shamiryan, S. De Gendt, M. Baklanov, *J. Appl. Phys.* **2010**, *107*, 104122.
[8] J. H. Yim, M. R. Baklanov, D. W. Gidley, H. Peng, H. D. Jeong, L. S. Pu, *J. Phys. Chem. B* **2004**, *108*, 8953.
[9] M. Darnon, T. Chevolleau, T. David, J. Ducote, N. Posseme, R. Bouyssou, F. Bailly, D. Perret, O. Joubert, *J. Vac. Sci. Technol., B* **2010**, *28*, 149.
[10] F. Lacopi, J. Choi, K. Terashima, P. Rice, G. Dubois, *Phys. Chem. Chem. Phys.* **2011**, *13*, 3634.
[11] A. Bhanap, B. Korolev, S. Nitta, S. Purushothaman, G. Bonilla, E. T. Ryan, *Solid State Technol.* **2007**, *50*, 79.
[12] V. Jousseaume, L. Favennec, A. Zenasni, G. Passemard, *Appl. Phys. Lett.* **2006**, *88*, 182908.
[13] R. Hoofman, V. Nguyen, V. Arnal, M. Broekaart, L. Gosset, W. Besling, M. Fayolle, F. Iacopi, in *Dielectric films for advanced microelectronics*, (Eds: M. Baklanov, K. Maex, M. Green), Wiley, New York **2007**, p. 199.
[14] T. Frot, W. Volksen, T. Magbitang, D. Miller, S. Purushothaman, M. Lofaro, R. Bruce, G. Dubois, "Post Porosity Plasma Protection a new approach to integrate k < 2.2 porous ULK materials", presented at *IEEE Int. Interconnect Technol. Conf.*, Dresden, **8–12 May, 2011**.
[15] T. Frot, W. Volksen, S. Purushothaman, R. Bruce, G. Dubois, *Adv. Mater.* **2011**, *23*, 2828.
[16] N. Krins, M. Faustini, B. Louis, D. Grosso, *Chem. Mater.* **2010**, *22*, 6218.

[17] G. Dubois, W. Volksen, T. Magbitang, R. D. Miller, D. M. Gage, R. H. Dauskardt, *Adv. Mater.* **2007**, *19*, 3989.
[18] G. Dubois, W. Volksen, T. Magbitang, M. H. Sherwood, R. D. Miller, D. M. Gage, R. H. Dauskardt, *J. Sol-Gel Sci. Technol.* **2008**, *48*, 187.
[19] W. Volksen, T. P. Magbitang, R. D. Miller, S. Purushothaman, S. A. Cohen, H. Nakagawa, Y. Nobe, T. Kokubo, G. J. M. Dubois, *J. Electrochem. Soc.* **2011**, *158*, G155.
[20] W. Volksen, G. Dubois, T. Magbitang, T. Frot, P. Rice, L. Krupp, S. Purushothaman, R. L. Bruce, S. Cohen, M. Lofaro, S. U. Engelmann, H. Nakagawa, M. Sekiguchi, T. Kokubo, "Molecularly Reinforced Sol-Gel Glasses with Improved Pore Size Distribution", presented at *MRS Spring National Meeting*, San Francisco, **26-29 April 2011**.
[21] M. Oliver, G. Dubois, R. Dauskardt, "Molecular design of ultra-low-k hybrid glasses", presented at *IEEE Int. Interconnect Technol. Conf,* San Francisco **2010**.
[22] M. S. Oliver, G. Dubois, M. Sherwood, D. M. Gage, R. H. Dauskardt, *Adv. Funct. Mater.* **2010**, *20*, 2884.
[23] M. Baklanov, K. Mogilnikov, V. Polovinkin, F. Dultsev, *J. Vac. Sci. Technol. B* **2000**, *18*, 1385.
[24] K. Coakley, Y. Liu, M. McGehee, K. Frindell, G. Stucky, *Adv. Funct. Mater.* **2003**, *13*, 301.
[25] D. Ryu, K. Shin, E. Drockenmuller, C. Hawker, T. Russell, *Science* **2005**, *308*, 236.
[26] K. A. Barnes, A. Karim, J. F. Douglas, A. I. Nakatani, H. Gruell, E. J. Amis, *Macromolecules* **2000**, *33*, 4177.
[27] Y. Travaly, J. Schuhmacher, A. M. Hoyas, M. Van Hove, K. Maex, T. Abell, V. Sutcliffe, A. M. Jonas, *J. Appl. Phys.* **2005**, *97*, 084316.
[28] A. Grill, V. Patel, *J. Electrochem. Soc.* **2006**, *153*, F169.
[29] N. Posseme, R. Bouyssou, T. Chevolleau, T. David, V. Arnal, S. Chhun, C. Monget, E. Richard, D. Galpin, J. Guillan, "In situ post etching treatment as a solution to improve defect density for porous low-k integration using metallic hard masks", presented at *IEEE Int. Interconnect Technol. Conf.,* Sapporo, **1–3 June, 2009**.
[30] M. S. Kuo, G. Oehrlein, *J. Vac. Sci. Technol. B* **2010**, *28*, 1104.
[31] G. S. Oehrlein, R. J. Phaneuf, D. B. Graves, *J. Vac. Sci. Technol. B* **2011**, *29*, 010801.
[32] A. Urbanowicz, K. Vanstreels, P. Verdonck, D. Shamiryan, S. De Gendt, M. Baklanov, *J. Appl. Phys.* **2010**, *107*, 104122.
[33] E. T. Ryan, S. M. Gates, A. Grill, S. Molis, P. Flaitz, J. Arnold, M. Sankarapandian, S. A. Cohen, Y. Ostrovski, C. Dimitrakopoulos, *J. Appl. Phys.* **2008**, *104*, 094109.